ANALYSIS OF RESONANCE EXCITATION AND SURFACE DISTORTION OF SINGLE MICRODROPLETS USING FOCUSED MONOCHROMATIC ILLUMINATION

FINAL REPORT

MARCH 15, 1999

PRINCIPAL INVESTIGATOR
Dr. John P. Barton, Associate Professor
Department of Mechanical Engineering
College of Engineering & Technology
University of Nebraska-Lincoln
Lincoln, Nebraska 68588-0656
Ph# (402) 472-5081
Fax# (402) 472-1465
Email jbarton@unlinfo.unl.edu

SPONSORING AGENCY
Department of the Navy
Naval Research Laboratory
4555 Overlook Avenue, SW
Washington, DC 20375-5326
Program Officer: Dr. Anthony J. Campillo
Grant No. N00173-98-1-G008
PR No. 56-9117-98

"Analysis of Resonance Excitation and Surface Distortion
of Single Microdroplets Using Focused Monochromatic Illumination"

John P. Barton
University of Nebraska-Lincoln
March 15, 1999

I. Introduction

Theoretical procedures were developed, computer programs were written, and systematic calculations were performed to investigate (1) the validity of the van de Hulst's localization principle for spherical and nonspherical particles and (2) the effects of laser beam induced electromagnetic stresses on droplet geometry. The results of this study are described in the following. Section II contains the results of a systematic investigation, for the arrangement of a focused laser beam incident upon a spherical particle, of the validity of the localization principle as a function of beam waist diameter and resonance mode conditions. In Sec. III., the effects of surface perturbations on the validity of the localization principle and resonance Q are discussed. Section IV provides calculated electromagnetic stress distributions for a spherical particle at resonance and nonresonance conditions. In Sec. V, the theoretical development for the determination of the effects of electromagnetically-induced stresses on droplet geometry is presented along with some initial calculated results. A discussion of possible future work is given in Sec. VI.

II. Localization Principle: Resonance Mode and Beam Waist Effects

A set of systematic calculations were performed investigating the validity of van de Hulst's localization principle as a function of beam waist diameter and resonance mode. The van de Hulst's localization principle predicts that a spherical particle resonance should be most strongly excited with the laser beam focused at a radial position (r_0) given by

$$r_0/a = (l + 1/2)/\alpha \tag{1}$$

where a is the particle radius, l is the resonance principle mode number and $\alpha = 2\pi a/\lambda_{ext}$ is the particle size parameter. Since under ordinary circumstances $l > \alpha$, Eq. (1) suggests that the resonance will be most strongly excited by positioning the focal point of the incident laser beam outside the surface of the particle. To test the rigor of Eq. (1), calculations of resonance excitation as a function of focal point positioning were performed for a range of different beam waist diameters and different resonance modes. The degree of resonance excitation was expressed by summing over the squares of the magnitudes of all the azimuthal mode (m terms) coefficients associated with the principle mode number (l, see Appendix A for details) which provides a single scalar term (U) that is proportional to the resonance electromagnetic energy stored in the particle.

The eight different resonance modes that were investigated are listed in Table I. along with the associated size parameter (α_0), resonance Q, and the localization principle prediction (r_0/a) for each resonance. For all except the $d_{97,2*}$ resonance, an index of refraction of $n =$ (1.332,0.0), approximately that of water at the argon-ion laser wavelength of 0.5145 μm, was assumed. For the special case of the $d_{97,2*}$ resonance, an index of refraction of (1.50,0.0) was

assumed. All resonances are magnetic wave (i.e., TE, transverse electric) resonances except for the $c_{97,1}$ resonance which is an electric wave (i.e., TM, transverse magnetic) resonance. The first subscript refers to the principle mode number of the resonance, while the second subscript refers to the order of occurrence of the resonance. The first five resonances listed in Table I, with size parameters of the order of 80, would correspond to the arrangement of an argon-ion laser incident upon an approximately 12 μm diameter water droplet. The last three resonances listed in Table I, with higher size parameters, would correspond to droplets with proportionally larger diameters.

A focused Gaussian beam propagating in the +z-axis direction and with electric field polarization in the x-axis direction was used to investigate the validity of the localization principle. For this arrangement, the magnetic wave resonances are most effectively excited by translating the focal point of the beam along the y-axis (incident electric field parallel to the particle surface). Figures 1, 2, and 3 show resonance excitation as a function of nondimensionalized beam focal point positioning along the y-axis (as given by $\tilde{y}_0 = y_0/a$) and nondimensionalized beam waist radius (as given by $\tilde{w}_0 = w_0/a$) for, respectively, the $d_{97,1}$, $d_{94,2}$, and $d_{91,3}$ resonances. As can be seen in Figs. 1-3, indeed, consistent with the localization principle, for equal power beams, a resonance can be most efficiently excited using a tightly focused beam with the focal point oriented just outside the surface of the particle at a location approximately equal to, but not exactly equal to, a location as predicted by the van de Hulst's localization principle. Figures 1-3 also show that the position for optimum resonance excitation depends not only on the principle mode number but on the relative beam waist radius as well.

The effect of beam waist radius on optimum focal point positioning is shown in Fig. 4. The horizontal dashed lines indicate the corresponding predicted values of of the localization principle. As can be seen in Fig. 4, for the $d_{97,1}$, $d_{94,2}$, and $d_{91,3}$ resonances, the optimum position for resonance excitation equals the localization principle prediction only when the beam waist is equal to about one-fifth of the particle diameter. For smaller beam waists the optimum focal point position is further from the particle than the predicted value and for larger beam waists the predicted value is closer to the particle than the predicted value.

In Fig. 5, a plot is presented of $\Delta y_0/a = y_0/a - r_0/a$ (the difference between the calculated focal point location for optimum resonance excitation and the the location as predicted by the localization principle) versus w_0/a (beam waist radius) for all eight of the different resonance modes. (For the $c_{97,1}$ mode, a focused beam with an electric field polarization in the y-axis direction was used.) As can be seen in Fig. 5, when $\Delta y_0/a$ is plotted versus w_0/a, the data clusters near a common line for w_0/a greater than about 0.20, but diverges for w_0/a less than about 0.20. Figure 6 is similar to Fig. 5, but now $\Delta y_0/a$ is plotted versus the product of the size parameter (α_0) and the beam waist radius (w_0/a). As can be observed in Fig. 6, when plotted in this way, the data clusters near a common line for w_0/a less than about 0.20, but diverges for w_0/a greater than about 0.20. From the results of Figs. 5 and 6, the following empirical relationship was derived and is offered a "corrected" version of the localization principle.

$$r_0/a = (l + 1/2)/\alpha + 1.08/(\alpha\tilde{w}_0)^2 - 0.099\tilde{w}_0^2 \qquad (2)$$

III. Localization Principle and Resonance Q: Surface Perturbation Effects

Systematic calculations, using the PI's boundary matching method, were performed investigating the effects of small surface perturbations on the resonance Q and the focused beam excitation of resonances in microspheres. The theoretical procedure and the calculated results are presented in a paper that was submitted to the Journal of the Optical Society of America A (subsequently, the paper was accepted for publication pending optional minor revision). A copy of the original manuscript of this paper, "The effects of surface perturbations on the quality (Q) and the focused beam excitation of microsphere resonance," is provided in Appendix A. The reader is referred to Appendix A for the details of this development, only a summary of the findings will be presented here.

The effects of perturbations on the same $d_{97,1}$, $d_{94,2}$, and $d_{91,3}$ magnetic wave resonances introduced in Sec. I (as well as the corresponding electric wave resonances, $c_{97,1}$, $c_{94,2}$, and $c_{91,3}$) were investigated. Axisymmetric particles with a "corrugated" roughness expressed by,

$$\hat{r}(\theta) = 1 + \epsilon \cos(N\theta) \quad , \tag{3}$$

where ϵ is the nondimensionalized (relative to the particle radius) amplitude of the perturbation and N was an integer that was varied through a range from 20 to 40, and a "combined" roughness expressed by,

$$\hat{r}(\theta) = 1 + \frac{\epsilon}{\sqrt{3}}[\cos(18\theta) + \cos(30\theta) + \cos(42\theta)] \quad , \tag{4}$$

were considered.

For a given resonance mode, the presence of a distributed surface perturbation was found to have a negligible effect on the resonance Q until a threshold value of surface perturbation amplitude (ϵ) is reached, after which the Q decreases with increasing ϵ (see, for example, App. A Figs. 2 and 4). The Q as a function of ϵ relationship was found to follow, for most cases, the simple second-power model suggested by Lai et al.,[1]

$$1/Q \approx 1/Q_{sp} + C_2\epsilon^2 \quad . \tag{5}$$

where Q_{sp} is the Q for the perfect sphere. However, for conditions that were weakly-Q spoiling, it was found necessary to include an additional fourth-power term. The excitation localization principle was found to fail when the surface roughness amplitude is large enough to cause a significant lowering of the resonance Q (see, for example, App. A Figs 5 and 6). In this case, for focused beam excitation of the resonance, the resonance was found to be most efficiently excited with the focal point of the beam located at a position just inside the surface of the particle. Apparently, for these conditions, the internal resonance mode is being pumped predominately by surface scattering due to the presence of the surface perturbations.

IV. Spherical Particle Electromagnetic Stress Distributions

The electromagnetic fields associated with a focused laser beam can induce stresses on a particle that may distort the particle shape and which, as shown in Sec. III, may

affect the resonance Q and the applicability of the localization principle. For a perfectly nonabsorbing particle (as considered here) the electromagnetically-induced stresses occur only at the surface of the particle, where the stress is directed outward and normal to the surface. For a liquid droplet, a nondimensional electromagnetic surface stress can be defined as,

$$\tilde{P} = \frac{r_0 P}{\sigma} \quad , \tag{6}$$

where, here, r_0 is the nominal droplet radius, P is the electromagnetic surface stress, and σ is the surface tension of the liquid-surrounding medium interface. $\tilde{P}$ can, in turn, be related to the electromagnetic fields by,

$$\tilde{P}(\theta) = \tilde{I}_0 F(\theta) \tag{7}$$

where

$$F(\theta) = \frac{1}{2}\epsilon_{ext}(n^2 - 1)[n^2 \tilde{E}_n^2 + \tilde{E}_{p,1}^2 + \tilde{E}_{p,2}^2]_{int} \tag{8}$$

and

$$\tilde{I}_0 = \frac{r_0 I_0}{\sigma c \sqrt{\epsilon_{ext}}} \tag{9}$$

In Eq. (8), $\tilde{E}_n^2, \tilde{E}_{p,1}^2$, and $\tilde{E}_{p,2}^2$ are, respectively, the nondimensionalized normal and two parallel components of the electric field at the particle surface (for a spherical particle, these would be $\tilde{E}_r^2, \tilde{E}_\theta^2$, and $\tilde{E}_\phi^2$) and in Eq. (9), I_0, is the nominal intensity of the incident beam. For example, for a water droplet in air ($\sigma \approx 0.0727\ N/m$ at $20°C$) with $d_0 = 2r_0 = 10\ \mu m$ and $I_0 = 1{\times}10^6\ W/cm^2$, $\tilde{I}_0 \approx 2.3{\times}10^{-3}$.

In order to demonstrate the distribution of electromagnetic stresses that might occur over the surface of a spherical droplet, calculations were performed for both nonresonance (α = 80) and resonance ($d_{97,1}$) conditions. Figures 7-10 show the angular distribution of $F(\theta)$ for plane wave incidence (propagating in the +z-axis direction) with electric field polarization in the x-axis direction. Figures 7 and 8 are for nonresonance, with Fig. 7 showing the distribution in the y-z plane and Fig. 8 showing the distribution in the x-z plane. The beam propagation direction is from left-to-right. As can be seen in Figs. 7 and 8, the focusing effect of the illuminated side of the droplet results in strong electric fields, and strong electromagnetic stresses, on the shadow side of the droplet. The stress distributions in the x-z and y-z planes are similar, but not identical, due to secondary polarization effects, and would tend to pull the droplet into a prolate-like geometry.

Figures 9 and 10 show the corresponding results for the $d_{97,1}$ resonance condition. In this case the electromagnetic stresses are greatly enhanced due to the resonance condition (the stress distributions of Figs. 9 and 10 have been scaled down by about 6 orders of magnitude in comparison with the stress distributions of Figs. 7 and 8). In addition, the stress distribution for the resonance condition, instead of being approximately axisymmetric as for the nonresonance condition, is now very nonaxisymmetric with the electromagnetic stresses concentrated in the y-z plane (the plane of the resonance). Figures 11 and 12 are for the same resonance condition as Figs. 9 and 10, but now a focused beam oriented at the surface of the droplet is used to excite the resonance (instead of plane wave incidence as used in Figs. 9 and 10). In this case, the light circles inside the particle in only one direction,

there are no interference effects, and the resultant electromagnetic stress is nearly uniform in the y-z plane. The stress distribution of Figs. 11 and 12 would tend to pull the droplet into an oblate-like geometry.

V. Electromagnetically-Induced Droplet Shape Distortion

The electromagnetically-induced stress distributions calculated in Sec. IV were for a spherical particle. For the case of a liquid droplet, the electromagnetically-induced surface stresses would distort the shape of the droplet. An iterative procedure was developed to determine the steady-state (i.e., equilibrium) geometry of a liquid droplet during continuous illumination by a high intensity laser beam. For the initial analysis, the incident light was assumed to be a circularly-polarized plane wave so that the electromagnetically-induced stresses, and thus the resultant droplet geometry as well, would be axisymmetric.

On the droplet surface, the electromagnetically-induced stresses are balanced by the surface tension stress and the pressure difference across the liquid interface,

$$-\sigma(\frac{1}{R_1}+\frac{1}{R_2}) = \Delta p(\theta) + P(\theta) \tag{10}$$

where R_1 and R_2 are the radius of curvatures of the surface, Δp is the pressure difference, and P is the electromagnetically-induced surface stress that was discussed in Sec. IV. If r_p represents the angular dependent radial coordinate position of the droplet surface, then for the axisymmetric geometry considered here, $r_p(\theta)$ only, and

$$\frac{1}{R_1} = -\frac{1}{r_p}\{1 - \frac{r_p''}{1+(r_p')^2}\} \tag{11}$$

and

$$\frac{1}{R_2} = -\frac{[1 - r_p' cos\theta/sin\theta]}{r_p\sqrt{1+(r_p')^2}} \tag{12}$$

where

$$r_p' = (\frac{1}{r_p}\frac{dr_p}{d\theta}) \tag{13}$$

and

$$r_p'' = \frac{d}{d\theta}(\frac{1}{r_p}\frac{dr_p}{d\theta}) \quad . \tag{14}$$

If $r_p = r_0(1+\epsilon)$ where $\epsilon(\theta)$ only (ϵ becomes the deviation of the droplet surface from that of a perfect sphere), then equivalently

$$r_p' = \frac{1}{r_p}\frac{\partial r_p}{\partial\theta} = \frac{\epsilon'}{(1+\epsilon)} \tag{15}$$

and

$$r_p'' = \frac{d}{d\theta}(\frac{1}{r_p}\frac{dr_p}{d\theta}) = \frac{\epsilon''}{(1+\epsilon)} - \frac{(\epsilon')^2}{(1+\epsilon)^2} \Rightarrow \frac{\epsilon''}{(1+\epsilon)} \tag{16}$$

where $\epsilon' = d\epsilon/d\theta$, $\epsilon'' = d^2\epsilon/d\theta^2$ and in Eq. (16) the assumption is made that $(\epsilon')^2 << 1$. When Eqs. (15) and (16) are used to eliminate r_p in terms of ϵ, Eqs. (11) and (12) give

$$-(\frac{1}{R_1}+\frac{1}{R_2}) = \frac{1}{r_0(1+\epsilon)^2}\{2+2\epsilon-\epsilon' cos\,\theta/sin\,\theta-\epsilon''\} \quad . \tag{17}$$

Now substituting Eq. (17) into Eq. (10), the following nondimensional equation can be obtained

$$\frac{1}{(1+\epsilon)^2}\{2+2\epsilon-\epsilon' cos\,\theta/sin\,\theta-\epsilon''\} = \Delta\tilde{p}+\tilde{P} \tag{18}$$

where $\Delta\tilde{p} = r_0\Delta p/\sigma$ and $\tilde{P} = r_0 P/\sigma$. Multiplying through by $(1+\epsilon)^2$, neglecting terms of the order of $(\epsilon)^2$, and rearranging gives

$$[2(\Delta\tilde{p}_0+\tilde{P}-1)-3\tilde{\gamma}cos\,\theta]\epsilon+[\frac{cos\,\theta}{sin\,\theta}]\epsilon'+\epsilon'' = 2-(\Delta\tilde{p}_0+\tilde{P})+\tilde{\gamma}cos\,\theta \tag{19}$$

where

$$\Delta\tilde{p} = \Delta\tilde{p}_0-\tilde{\gamma}(1+\epsilon)cos\,\theta \tag{20}$$

In Eq. (20), $\Delta\tilde{p}_0 = r_0 p_0/\sigma$ is the uniform part of the pressure difference (equal to 2 for a spherical droplet with no applied surface stresses) and $\tilde{\gamma} = \gamma r_0^2/\sigma$ is a pressure gradient term that may arise because of gravitation or the acceleration of the particle due to a net electromagnetic force.

The solution procedure for determining the steady-state geometry of a liquid droplet continuously illuminated by a high intensity laser beam is then as follows.
(1.) Assuming a perfectly spherical droplet, the nondimensionalized electromagnetically-induced surface stress distribution, $\tilde{P}(\theta)$, is calculated using the procedure discussed in Sec. IV.
(2.) $\tilde{P}(\theta)$ is then substituted into Eq. (19), and the deviation of the droplet geometry from the spherical geometry, $\epsilon(\theta)$, is determined by solving Eq. (19) using finite difference with the two boundary conditions that $\epsilon'(0) = 0$ and $\epsilon'(\pi) = 0$. In actual practice, for M increments, the conditions $\epsilon_0' = 0$ and $\epsilon_M = \epsilon_0$ were first imposed and then the values of $\Delta\tilde{p}_0$ and $\tilde{\gamma}$ were varied until the conditions of conservation of droplet volume, $\tilde{V} = V/\frac{4}{3}\pi r_0^3 = 1$, and $\epsilon_M' = 0$ were achieved.
(3.) The new droplet geometry as described by the $\epsilon(\theta)$ values obtained in Step 2 are now used to recalculate the electromagnetic field distribution and the corresponding electromagnetically-induced stress distribution, $\tilde{P}(\theta)$.
(4.) Steps 2 and 3 are now repeated until a convergence in $\epsilon(\theta)$ is obtained.

As an example, Fig. 13 shows the calculated droplet geometry (the value of ϵ has been doubled to assist visualization) for the nonresonance condition ($\alpha = 80$) with $\tilde{I}_0 = 0.05$. For this case it was found that $\tilde{\Delta}p_0 = 1.979$ (indicating a slight lowering of the internal pressure of the droplet) and $\tilde{\gamma} = 8.95 \times 10^{-3}$ (indicating a net force on the droplet in the +z-axis direction). As can be seen in Fig. 13, the strong electromagnetic stresses on the shadow side of the droplet (refer back to Figs. 7 and 8) elongate the droplet along the z-axis (i.e., prolate-like, but not symmetrical from front-to-back). Figure 14 is for the same conditions as Fig. 13, but now the incident intensity has been doubled to $\tilde{I}_0 = 0.10$. For $\tilde{I}_0 = 0.10$, $\Delta\tilde{p}_0$

$= 1.967$ (i.e., the internal pressure decreases) and $\tilde{\gamma} = 1.19 \times 10^{-2}$ (i.e., the pressure gradient increases). In addition, for the higher intensity, as seen in Fig. 14, the droplet distortion becomes more pronounced and the deviation from the initial spherical shape becomes more appreciable.

Some preliminary calculations have also been performed for the $d_{97,1}$ resonance condition. For this case the electromagnetic stresses are about six orders of magnitude greater than those of the nonresonance case and an $\tilde{I}_0 = 1 \times 10^{-7}$ was used. Even for this small of incident intensity, the first iteration showed that the droplet distortion would cause the droplet to be shifted away from resonance. More extensive calculations of droplet distortion at resonance are still in progress.

VI. Future Work

A partial list of future work is as follows.
1.) Organize the material in Sec II concerning the influence of beam waist and resonance mode on the localization principle, write up in manuscript form, and submit for publication.
2.) The boundary matching method was used for the surface perturbation effects on resonance Q and focus beam resonance excitation investigation. Since it was subsequently discovered that even small surface perturbations (i.e., $\epsilon < 0.005$) could create significant effects, a simpler/faster perturbation method might be used instead of the rigorous (but slower) boundary matching method.
3.) With regard to the effects of surface perturbations on resonance Q and focused beam resonance excitation, further systematic calculations are needed to a.) develop a better understanding of the grating effect, b.) investigate the effects of additional types of surface roughness, c.) investigate the effects at higher size parameters, and d.) compare with (or suggest) corresponding experimental measurements.
4.) The electromagnetically-induced droplet distortion work is still very much in its infancy and much more can be done including a.) consider the possibility of using the perturbation method instead of the boundary matching method for determining the electromagnetic fields of the distorted droplet (at least for the cases where the surface distortion is slight, b.) automate the iteration procedure (at this point, several decision steps of the iteration procedure are performed by the user), c.) revise the finite difference procedure to relax the $\epsilon^2 << 1$ assumption, d.) perform systematic calculations for droplets at resonance, e.) seek experimental confirmation of the predicted results, and f.) write up the initial work into manuscript form and submit for publication.

References

1. H.M. Lai, C.C. Lam, P.T. Leung, and K. Young, "Effect of perturbations on the widths of narrow morphology-dependent resonances in Mie scattering," J. Opt. Soc. Am. B **8**, 1962-1973 (1991).

Table I. Size parameter (α_0), resonance Q, and van de Hulst's localization principle prediction (r_0/a) for eight different resonance modes. Plane wave propagating in the +z-axis direction with electric field polarization in the +x-axis direction. Relative index of refraction of n = (1.332,0.000) for all resonance modes except the $d_{97,2*}$ mode where a relative index of refraction of n = (1.500,0.000) is assumed.

resonance mode	α_0	Q	r_0/a
$d_{97,1}$	78.557854283	1.419E+09	1.24112
$d_{94,2}$	81.25576849	1.207E+06	1.16299
$d_{91,3}$	83.0653044	1.160E+04	1.10154
$d_{97,2^*}$	78.254645969	3.550E+09	1.24593
$c_{97,1}$	79.0183692517	1.006E+09	1.23389
$d_{136,2}$	114.2196079147	6.61E+09	1.19507
$d_{142,3}$	123.681366193	7.92E+07	1.15215
$d_{180,5}$	158.199397181	7.330E+08	1.14097

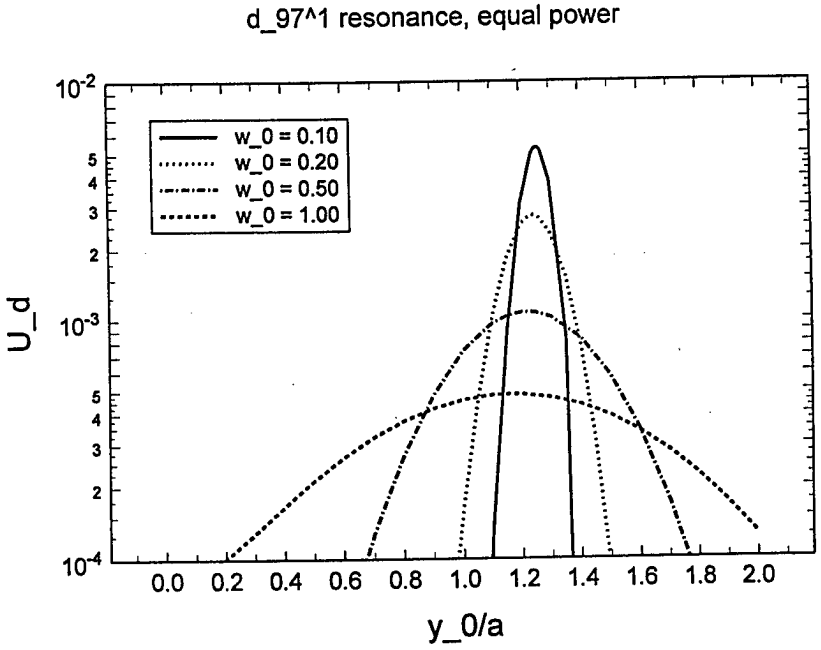

FIG 1. Electromagnetic energy versus beam focal point location for equal power beams with differing beam waist radius. $d_{97,1}$ resonance.

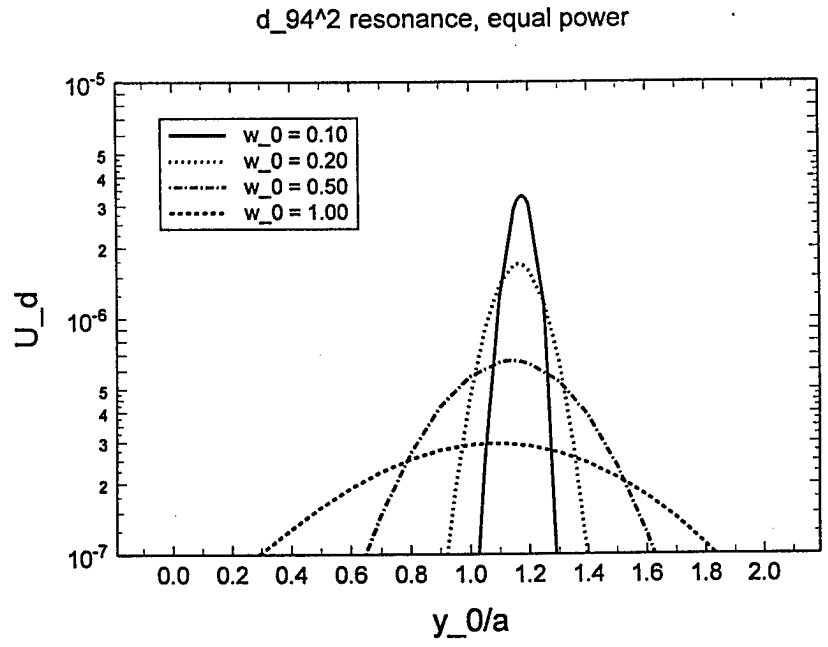

FIG 2. Electromagnetic energy versus beam focal point location for equal power beams with differing beam waist radius. $d_{94,2}$ resonance.

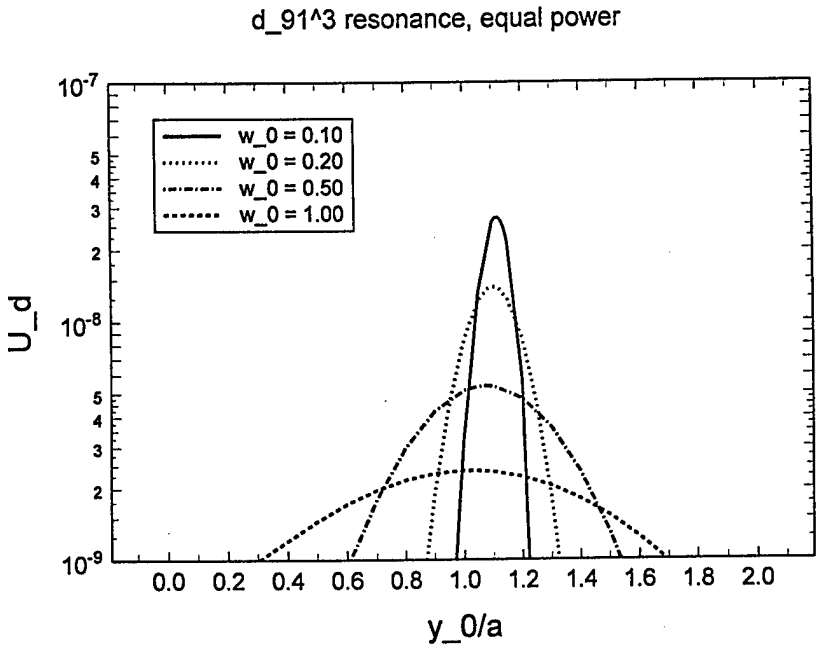

FIG 3. Electromagnetic energy versus beam focal point location for equal power beams with differing beam waist radius. $d_{91,3}$ resonance.

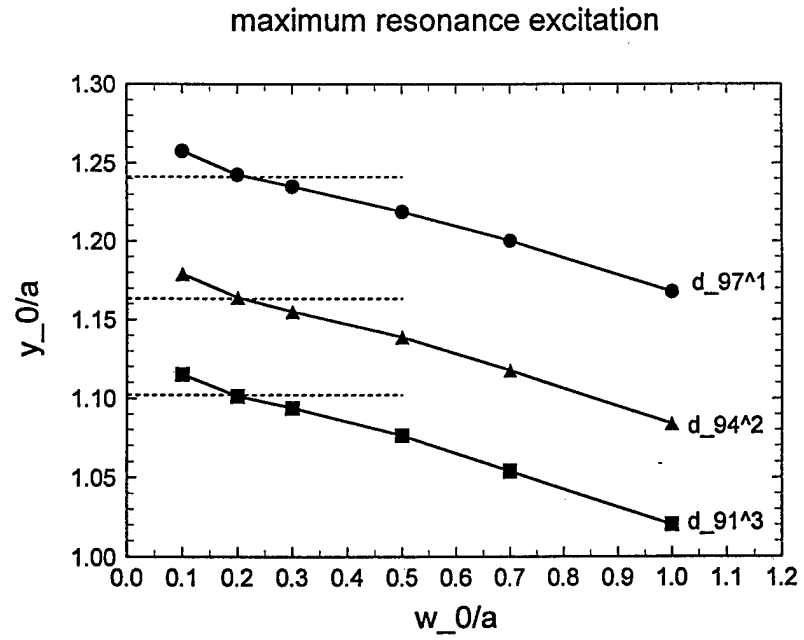

FIG 4. Location for maximum resonance excitation as a function of beam waist radius for the $d_{97,1}$, $d_{94,2}$, and $d_{91,3}$ resonances. Van de Hulst's localization principle prediction values shown as horizontal dashed lines.

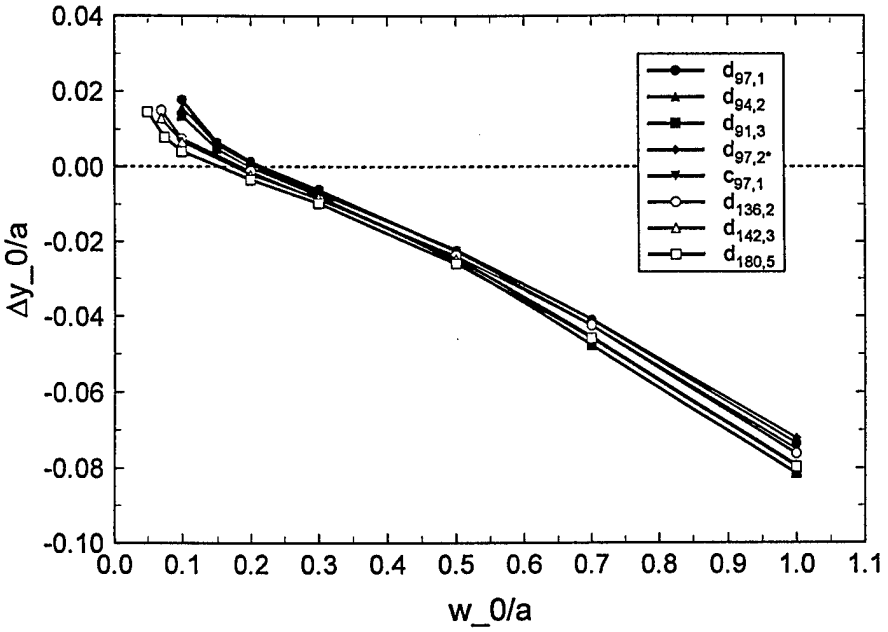

FIG 5. Difference between calculated location for maximum resonance excitation and the corresponding localization principle prediction ($\Delta y_0/a$) versus beam waist radius (w_0/a) for each of the eight different resonance modes.

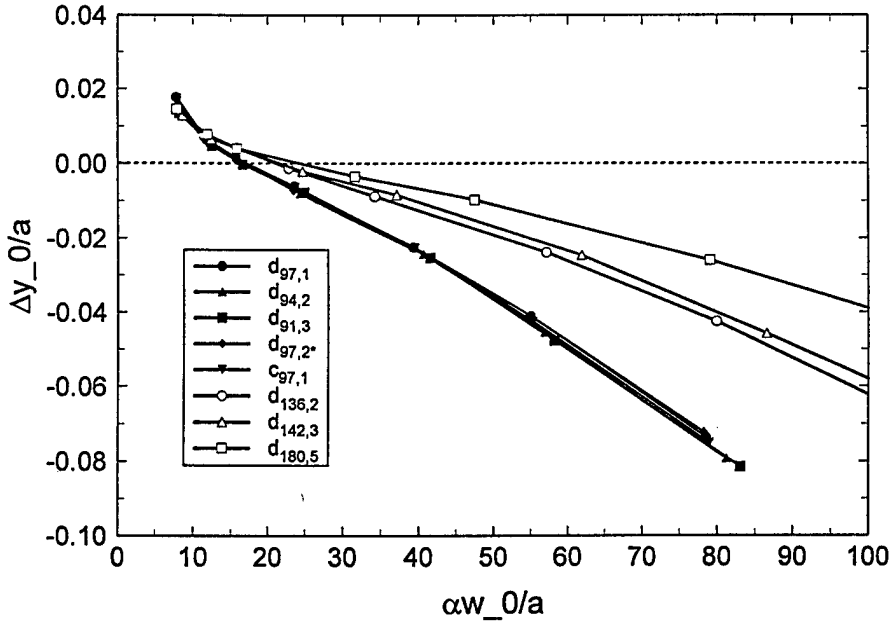

FIG 6. Difference between calculated location for maximum resonance excitation and the corresponding localization principle prediction ($\Delta y_0/a$) versus the product of size parameter and beam waist radius ($\alpha w_0/a$) for each of the eight different resonance modes.

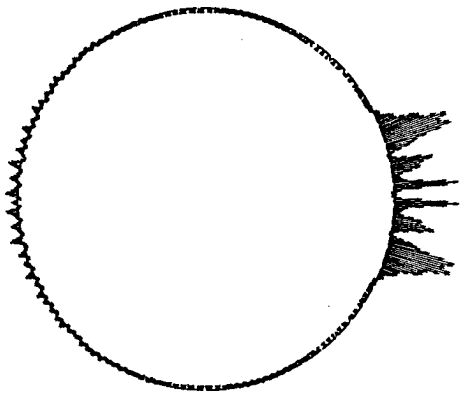

FIG 7. Electromagnetic stress distribution, $F(\theta)$, in the y-z plane for plane wave incidence (left-to-right) on a spherical particle at nonresonance ($\alpha = 80$). Electric field polarization in the x-axis direction.

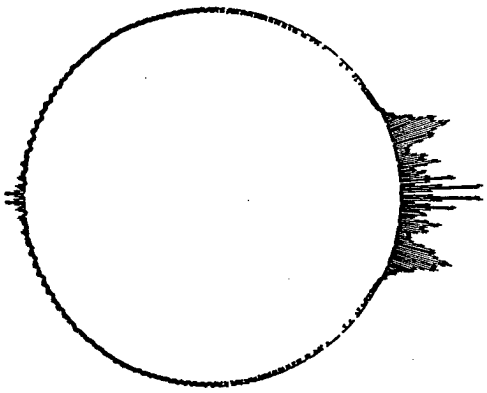

FIG 8. Electromagnetic stress distribution, $F(\theta)$, in the x-z plane for plane wave incidence (left-to-right) on a spherical particle at nonresonance ($\alpha = 80$). Electric field polarization in the x-axis direction.

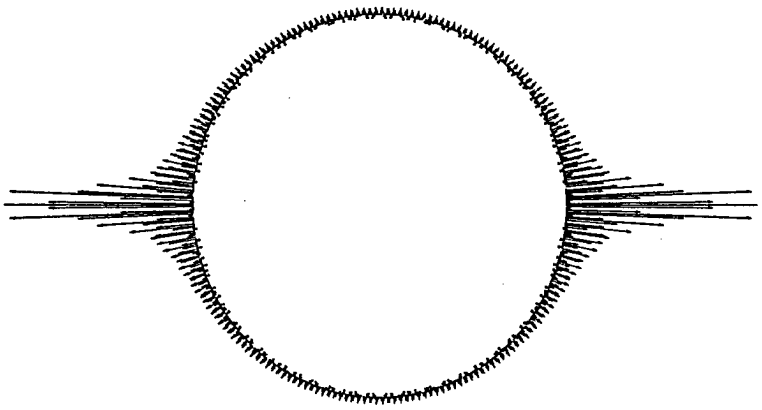

FIG 9. Electromagnetic stress distribution, $F(\theta)$, in the y-z plane for plane wave incidence (left-to-right) on a spherical particle at resonance ($d_{97,1}$). Electric field polarization in the x-axis direction.

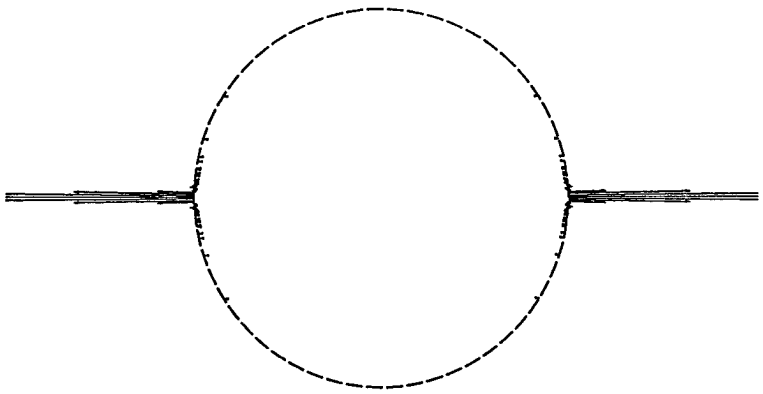

FIG 10. Electromagnetic stress distribution, $F(\theta)$, in the x-z plane for plane wave incidence (left-to-right) on a spherical particle at resonance ($d_{97,1}$). Electric field polarization in the x-axis direction.

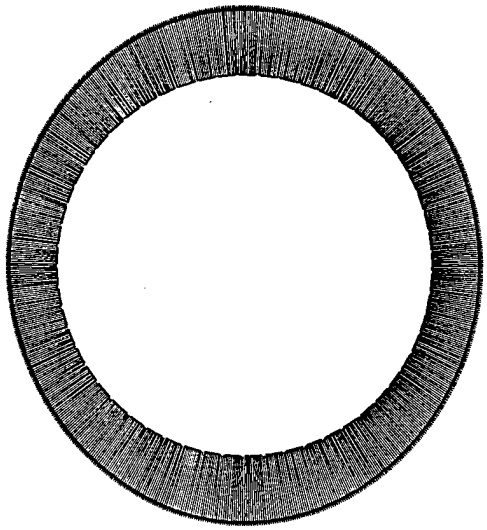

FIG 11. Electromagnetic stress distribution, $F(\theta)$, in the y-z plane for focused beam incidence (left-to-right, focal point positioning at the surface of the droplet) on a spherical particle at resonance ($d_{97,1}$). Electric field polarization in the x-axis direction.

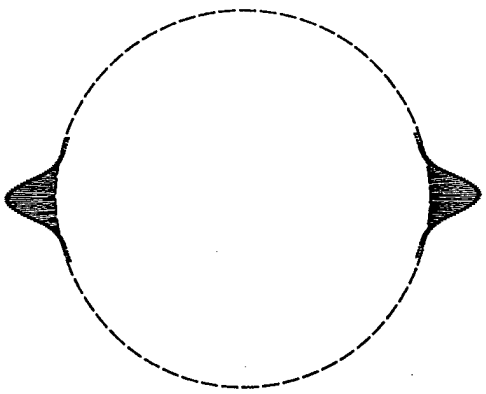

FIG 12. Electromagnetic stress distribution, $F(\theta)$, in the x-z plane for focused beam incidence (left-to-right, focal point positioning at the surface of the droplet) on a spherical particle at resonance ($d_{97,1}$). Electric field polarization in the x-axis direction.

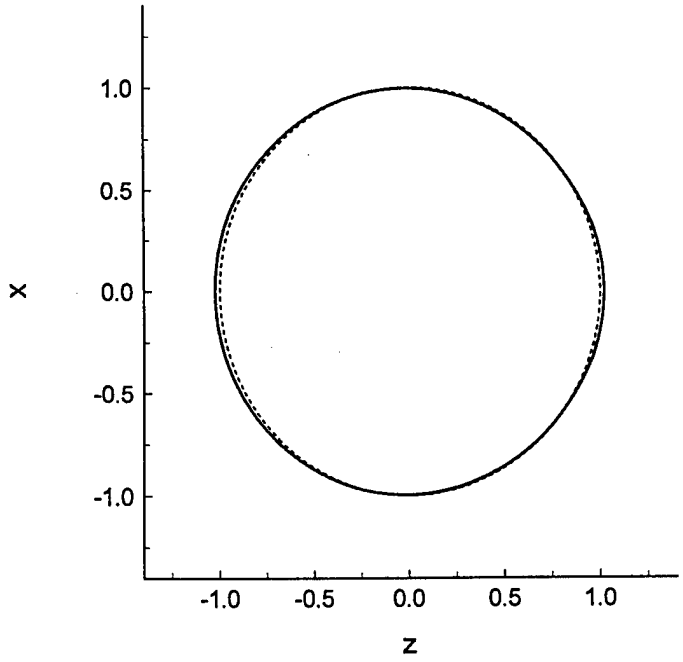

FIG 13. Calculated geometry of a nonresonance droplet ($\alpha = 80$). $\tilde{I}_0 = 0.05$, $\Delta\tilde{p}_0 = 1.979$, and $\tilde{\gamma} = 8.95 \times 10^{-3}$. The value of ϵ has been doubled to assist in visualization of the shape distortion.

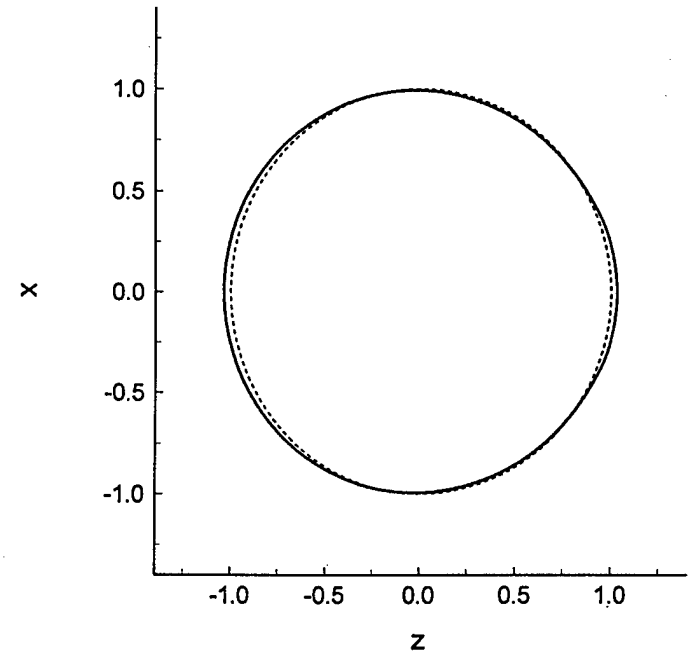

FIG 14. Calculated geometry of a nonresonance droplet ($\alpha = 80$). $\tilde{I}_0 = 0.10$, $\Delta\tilde{p}_0 = 1.967$, and $\tilde{\gamma} = 1.19 \times 10^{-2}$. The value of ϵ has been doubled to assist in visualization of the shape distortion.

APPENDIX A

"The effects of surface perturbations on the quality (Q)
and the focused beam excitation of microsphere resonance"

A paper accepted for publication (with optional minor revisions)
in the Journal of the Optical Society of America A.

"The effects of surface perturbations on the quality (Q) and the focused beam excitation of microsphere resonance"

John P. Barton
Department of Mechanical Engineering
College of Engineering & Technology
University of Nebraska-Lincoln
Lincoln, Nebraska 68588-0656

Abstract

A previously developed theoretical method for determining the electromagnetic fields for arbitrary monochromatic light incident upon an irregularly-shaped particle, the boundary matching method, was used to investigate the effects of small surface perturbations on the quality (Q) and the focused beam excitation of resonances in microspheres. Axisymmetric particles with periodic surface roughness and irregular surface roughness were considered. For a given resonance, the resonance Q was found to be relatively unaffected by the presence of the surface perturbations until the surface perturbation amplitude (ϵ) reached a threshold value, beyond which the Q decreases rapidly with increasing ϵ. For the perfect sphere, focused beam excitation of the resonance is most efficient with the beam focused outside the surface of the sphere, at a location consistent with the prediction of van de Hulst's localization principle. However, calculations indicate that for conditions where the surface perturbation amplitude is large enough to appreciably decrease the resonance Q, focused beam excitation of the resonance is most efficient with the beam focused just inside the particle surface.

1. Introduction

Solutions to the classical problem of the electromagnetic interaction of a monochromatic plane wave with a homogeneous, perfectly spherical particle, known as Lorenz-Mie theory, suggests that a micron-sized particle, in the absence of significant absorption, is capable of sustaining resonances of extremely high quality (resonance quality factor = Q = $\omega_0 U_0 / P_{loss}$ where ω_0 = the angular frequency, U_0 = the electromagnetic energy stored, and P_{loss} = the electromagnetic power loss due to absorption and scattering). For example, calculations indicate that a 30 micron diameter spherical particle with a relative index of refraction of 1.332 and an illuminating wavelength of approximately 0.5 microns can exhibit first-order resonances with Q values exceeding 10^{24}. (See Appendix A for details.) In fact, such high Q values have not been experimentally observed, either for solid (fused-silica) spheres[1,2] or for liquid droplets.[3–5] Maximum experimentally observed Q values have been less than 10^{10}. Absorption alone is not sufficient to explain the lowered Q values, and the additional lowering of the resonance Q has been attributed to increased surface scattering due to the presence of small shape distortions and surface irregularities of the particle.[1–5]

Theoretical calculations for a focused laser beam incident upon a perfect sphere have also predicted, consistent with the van de Hulst's localization principle,[6] that resonances should be most effectively excited by focusing the laser beam at a location outside the surface of the sphere, the location of optimum resonance excitation being equal to approximately[7,8]

$$r_o/a = (l + 1/2)/\alpha_o \qquad (1)$$

where a is the radius of the sphere, l is the principal mode number of the resonance, and $\alpha_o = 2\pi a/\lambda_{ext}$ is the particle size parameter for the resonance. In a recent publication,[9] it was reported that efforts to experimentally verify the excitation localization principle, as expressed by Eq. (1), were not successful for the case of quartz (i.e., solid) spheres, and for the case of liquid droplets the excitation localization principle was observed for some resonances, but not observed for others. Theoretical calculations, to be further discussed and expanded upon here, suggested that the presence of surface roughness, even to the order of molecular scale roughness, would explain the lack of experimental confirmation of the excitation localization principle.

In this paper, a previously developed theoretical method for determining the electromagnetic fields associated with the interaction of arbitrary monochromatic light with an irregularly-shaped homogeneous particle, referred to as the boundary matching method,[10] is used to systematically investigate the effects of small surface perturbations on the Q and the focused beamed excitation of resonances in microspheres. In Ref. 10, as a demonstration of the applicability of the boundary matching method, preliminary calculations were presented showing the effects of a single localized axisymmetric surface deformation on one particular microsphere resonance. In the following, the effects of roughness distributed over the entire surface of the sphere is considered for several different types of resonances. Other researchers, using various approaches, have also considered the effects of surface perturbations on the quality of microsphere resonance,[11–15] but their presented results were limited to low order (e.g., near prolate or near oblate) surface distortions and not the higher-order distributed surface roughness considered here. In addition, these researchers did not consider, as is presented in this paper, the possible effects of surface perturbations on the excitation localization principle.

2. Theoretical Development

A detailed description of the boundary matching method can be found in Ref. 10. Only a general overview and prerequisite essentials are given here. The electromagnetic interaction of a known incident monochromatic field (plane wave, focused beam, etc.) with a homogeneous irregularly-shaped particle located within a homogeneous infinite medium is considered. Both the particle and the surrounding medium are nonmagnetic ($\mu = 1$), and an implicit time dependence of exp(-$i\omega t$) is assumed. A spherical coordinate system, (r, θ, ϕ), with the coordinate origin located near the center of the particle is utilized. All equations are nondimensionalized with spatial quantities nondimensionalized relative to a characteristic radius, a, associated with the particle. The electromagnetic field components, $\vec{E}$ and $\vec{H}$, are nondimensionalized relative to a characteristic electric field value, E_0, associated with the incident field. The particle geometry is described by the particle radial shape function, $\hat{r}$, which is assumed to be a single valued function of angular position, (θ, ϕ). The incident field, designated by the superscript (i), is assumed known and the internal particle field, designated by the superscript (w), and the scattered field, designated by the superscript (s), are to be determined. The internal and scattered fields are each expressed in terms of general series expansions over appropriate products of spherical wave functions.[10] The series expansions for the field components of the internal field, of interest here, are as follows,

$$E_r^{(w)} = \frac{1}{\tilde{r}^2}\sum_{l=1}^{L}\sum_{m=-l}^{l}\left[l(l+1)\,c_{lm}\,\psi_l(\bar{n}\alpha\tilde{r})\,Y_{lm}(\theta,\phi)\right], \tag{2}$$

$$E_\theta^{(w)} = \frac{\alpha}{\tilde{r}}\sum_{l=1}^{L}\sum_{m=-l}^{l}\left[\bar{n}c_{lm}\,\psi_l'(\bar{n}\alpha\tilde{r})\frac{\partial Y_{lm}(\theta,\phi)}{\partial\theta} - \frac{m}{\sqrt{\epsilon_{ext}}}d_{lm}\,\psi_l(\bar{n}\alpha\tilde{r})\frac{Y_{lm}(\theta,\phi)}{\sin\theta}\right], \tag{3}$$

$$E_\phi^{(w)} = \frac{\alpha}{\tilde{r}}\sum_{l=1}^{L}\sum_{m=-l}^{l}\left[i\,m\,\bar{n}c_{lm}\,\psi_l'(\bar{n}\alpha\tilde{r})\frac{Y_{lm}(\theta,\phi)}{\sin\theta} - \frac{i}{\sqrt{\epsilon_{ext}}}d_{lm}\,\psi_l(\bar{n}\alpha\tilde{r})\frac{\partial Y_{lm}(\theta,\phi)}{\partial\theta}\right], \tag{4}$$

$$H_r^{(w)} = \frac{1}{\tilde{r}^2}\sum_{l=1}^{L}\sum_{m=-l}^{l}\left[l(l+1)\,d_{lm}\,\psi_l(\bar{n}\alpha\tilde{r})\,Y_{lm}(\theta,\phi)\right], \tag{5}$$

$$H_\theta^{(w)} = \frac{\alpha}{\tilde{r}}\sum_{l=1}^{L}\sum_{m=-l}^{l}\left[\bar{n}d_{lm}\,\psi_l'(\bar{n}\alpha\tilde{r})\frac{\partial Y_{lm}(\theta,\phi)}{\partial\theta} + m\sqrt{\epsilon_{ext}}\bar{n}^2 c_{lm}\,\psi_l(\bar{n}\alpha\tilde{r})\frac{Y_{lm}(\theta,\phi)}{\sin\theta}\right], \tag{6}$$

and

$$H_\phi^{(w)} = \frac{\alpha}{\tilde{r}}\sum_{l=1}^{L}\sum_{m=-l}^{l}\left[i\,m\,\bar{n}d_{lm}\,\psi_l'(\bar{n}\alpha\tilde{r})\frac{Y_{lm}(\theta,\phi)}{\sin\theta} + i\sqrt{\epsilon_{ext}}\bar{n}^2 c_{lm}\,\psi_l^{(1)}(\bar{n}\alpha\tilde{r})\frac{\partial Y_{lm}(\theta,\phi)}{\partial\theta}\right], \tag{7}$$

where $\tilde{r} = r/a$, l is the integer radial index, m is the integer angular index, ψ_l is the Riccati-Bessel function of the first kind, Y_{lm} is the spherical harmonic function, ϵ_{ext} is the dielectric constant of the external medium, and $\alpha = 2\pi a/\lambda_{ext}$ is the particle size parameter where λ_{ext} is the wavelength in the external medium. The upper limit of the radial index summation, L, is chosen sufficiently large so as to obtain the level of desired accuracy.

At the surface of the particle ($\tilde{r} = \hat{r}(\theta,\phi)$), the tangential components of the electric and magnetic fields are continuous,

$$\hat{n} \times (\vec{E}^{(i)} + \vec{E}^{(s)}) = \hat{n} \times \vec{E}^{(w)} \tag{8}$$

and

$$\hat{n} \times (\vec{H}^{(i)} + \vec{H}^{(s)}) = \hat{n} \times \vec{H}^{(w)} \tag{9}$$

where $\hat{n}$ is a unit vector perpendicular to, and outwardly directed from, the particle surface. Eqs. (8) and (9) are functions of (θ,ϕ) only, and can be expanded in spherical harmonics, and then matched mode-by-mode. The result is a set of simultaneous linear, algebraic equations that can be solved for the series coefficients of the scattered (a_{lm}, b_{lm}) and internal (c_{lm}, d_{lm}) fields. Once the series coefficients have been determined, the series expansions can be used to calculate the electromagnetic field components anywhere internal or external to the particle.

In general, the incident illumination (e.g., either a linearly polarized plane wave or focused Gaussian beam) is assumed to propagate parallel to the x-z plane with an angle of θ_{bd} relative to the y-z plane and with the direction of electric field polarization at an angle of ϕ_{bd} relative to the x-z plane (see Fig. 1) . For focused beam illumination, the beam waist radius, $\tilde{w}_0 = w_0/a$, and the position of the focal point relative to the coordinate origin, $(\tilde{x}_0, \tilde{y}_0, \tilde{z}_0) = (x_0/a, y_0/a, z_0/a)$, must also be specified.

For the external excitation of resonances, the presence of a particle resonance is evidenced by a sharp increase in the electromagnetic energy stored within the particle, U, where[16]

$$U = \frac{1}{16\pi}\int_V [Re(\epsilon_{ext}\bar{n}^2)|\vec{E}|^2 + |\vec{H}|^2]dV \quad . \tag{10}$$

For a perfectly spherical particle ($\hat{r} = 1$), Eqs. (2)-(9) can be used to substitute for $\vec{E}$ and $\vec{H}$ and Eq. (10) can be integrated analytically. One then finds (see Eqs. (18) and (19) in Ref. 16),

$$U = \sum_{l=1}^{L}\sum_{m=-l}^{l}[\,C_l|c_{lm}|^2 + D_l|d_{lm}|^2] \tag{11}$$

where C_l and D_l depend upon α, $\bar{n}$, and ϵ_{ext}, but **not** on the character of the incident field. According to Eq. (11), each internal field series coefficient contributes to U independently of the others, and, indeed, each resonance can be associated with the increase in magnitude of a particular series coefficient, either a c_{lm} coefficient for electric wave (TM) resonances or a d_{lm} coefficient for magnetic wave (TE) resonances where the value of l is the principal mode number of the resonance and the value of m is the azimuthal mode number of the resonance. For a spherical particle, for a given electric wave or magnetic wave resonance of principal mode number, l, the azimuthal (i.e., m) resonance modes are degenerate (occur at the same frequency), and U can be equivalently expressed as

$$U = \sum_{l=1}^{L}[\,C_l|c_l|^2 + D_l|d_l|^2] \tag{12}$$

where

$$|c_l|^2 = \sum_{m=-l}^{l}|c_{lm}|^2 \tag{13}$$

and

$$|d_l|^2 = \sum_{m=-l}^{l}|d_{lm}|^2 \quad . \tag{14}$$

Near a resonance, the $|c_l|^2$ and $|d_l|^2$ terms follow a Lorentzian profile, and the resonance quality factor, Q, can be determined using

$$Q = \frac{\alpha_o}{\Delta\alpha} \tag{15}$$

where α_o is the size parameter for the peak value and $\Delta\alpha$ is the full-width-half-maximum (FWHM) for the particular $|c_l|^2$ or $|d_l|^2$ term. Since each resonance term contributes independently to U, Eq. (15) can be used to determine the resonance quality independent of the type of incident field (plane wave, focused beam, etc.) being used to excite the resonance. One qualifying assumption associated with the use of Eq. (15), however, would be that the power (originating from the incident field) going in to the particular resonance term is constant over the width of the resonance ($\Delta\alpha$), which, in general, is a very good assumption, particularly for high Q resonances where $\Delta\alpha$ is small. (If the assumption is not valid, then the profile of $|c_l|^2$ or $|d_l|^2$ at resonance will not follow a symmetric Lorentzian profile, a criterion that can be checked at the time of calculation.)

In addition, for the perfectly spherical particle, as shown in Ref. 16, the internal field series coefficients (c_{lm}, d_{lm}) are directly related, mode-by-mode, to the corresponding incident field coefficients (A_{lm}, B_{lm}). That is, the value of c_{lm} is directly proportional to A_{lm} and the value of d_{lm} is directly proportional B_{lm} and there is no cross-coupling of terms (see Eqs. (12) and (13) in Ref. 16). For a perfectly spherical particle, a c_{lm} mode resonance will be excited only by the presence of a A_{lm} mode component of the incident field and, likewise, a d_{lm} mode resonance will be excited only by the presence of a B_{lm} mode component of the incident field. However, for the irregularly-shaped particle, this may well not be the case, since the simultaneous solution of the field equations permits a cross-coupling of terms and the excitation of a resonance may be obtained from incident field components of differing modes.

Also, as can be seen by eliminating A_{lm} and B_{lm} from Eqs. (10)-(13) in Ref. 16, for the perfectly spherical particle, the value of the a_{lm} scattered field series coefficient is directly proportional to the corresponding mode c_{lm} internal field coefficient and the b_{lm} scattered field coefficient is directly proportional to the corresponding mode d_{lm} internal field series coefficient. This implies, for a perfectly spherical particle, that a particular mode resonance (c_{lm} or d_{lm}) can only scatter into the same corresponding mode (a_{lm} or b_{lm}). Again, for the irregularly-shaped particle, this may not be the case. Because of the cross-coupling of terms, a particular mode resonance may scatter into any mode, which provides additional possible mechanisms for scattering losses not available for the perfect sphere resonance.

As was already demonstrated in Ref. 10 (refer to Figs. 13 and 14 in Ref. 10), the presence of a small surface deformation can create a shifting (change of α_0) and decay (increase of $\Delta\alpha$) for a given resonance term. The question now arises as to whether the procedure for identifying and determining the quality of resonances for a spherical particle is applicable for irregularly-shaped (i.e., nonspherical) particles. First, without the symmetry of the spherical particle, the azimuthal resonance modes of irregularly-shaped particles are not necessarily degenerate and each azimuthal mode will need to be individually identified and analyzed (i.e., Eq. (15) will be applied to $|c_{lm}|^2$ and $|d_{lm}|^2$, not to $|c_l|^2$ and $|d_l|^2$). Second, and more importantly, the total electromagnetic energy, as given by Eq. (10), for an irregularly-shaped particle with $\hat{r}(\theta, \phi) \neq 1$, is unlikely to lead, as was the case for the spherical particle, to the series form of Eq. (11). For a general irregularly-shaped particle the contribution of each internal field series coefficient to U would not necessarily be independent one from the other, and the quality of a resonance would have to be assessed using Eq. (15) on U, and not on individual terms. An exception would be, as considered here, spherical particles with small surface perturbations (in this case, less than 0.005 of a). Under these conditions, an evaluation of Eq. (10) from $0 \leq r \leq a$, leading to Eq. (11), would provide a good approximation for U. The spherical integration would include most of the particle volume ($> 99\%$) but would omit the parts of the particle where the perturbations are positive and would include parts of the surroundings where the perturbations are negative. Since the perturbation amplitudes are a fraction of a wavelength, the field energy would not be expected to vary appreciably over this region and, thus, the electromagnetic energy contributions of the included and excluded parts should be approximately equal, and the deviation from the correct value of U should be small. In addition, if the error in U using Eq. (11) is approximately constant over $\Delta\alpha$, then the values of α_0 and $\Delta\alpha$ will be unaffected and Q will be accurately determined, regardless of the error. In any event, for the calculations

that follow, Q values will be determined by applying Eq. (15) to individual $|c_{lm}|^2$ and $|d_{lm}|^2$ terms.

3. Surface Perturbation Effects on Q

Though the boundary matching method is applicable for general three dimensional particle geometries, the computational effort is significantly reduced if the particle is axisymmetric about the z-axis,[10] and only such axisymmetric geometries are considered. In addition, the resonances will be excited using a linearly polarized (electric field polarization parallel to the x-z plane, $\phi_{bd} = 0°$) plane wave with end-on ($\theta_{bd} = 0°$) incidence. For the axisymmetric particle with plane wave end-on incidence, only the $|m| = 1$ azimuthal modes are excited (i.e., all series coefficients with $|m| \neq 1$ are zero) so that, for a given magnetic wave or electric wave resonance at a particular principal mode number, only the single $|m| = 1$ azimuthal mode (the $m = +1$ and the $m = -1$ azimuthal modes are degenerate) will be observed.

For the initial calculations, surface roughness is modeled by assuming a corrugated particle geometry such that,

$$\hat{r}(\theta) = 1 + \epsilon \cos(N\theta), \tag{16}$$

where ϵ is the surface perturbation amplitude and N is an integer. A corrugated particle with N=20 is shown in Fig. 1. A relative index of refraction of $\bar{n} = n = 1.332$ (nonabsorbing), an external dielectric constant of $\epsilon_{ext} = 1$, and size parameters of the order of 80 were chosen so as to approximately model the experimental conditions of Ref. 9 (0.5145 micron argon-ion wavelength illumination of 10-16 micron diameter water droplets). Six different types of spherical particle resonances were identified for investigation: d^1_{97}, d^2_{94}, d^3_{91}, c^1_{97}, c^2_{94}, and c^3_{91} where the d indicates a magnetic wave (TE) resonance, the c indicates an electric wave (TM) resonance, the subscript is the principal mode number of the resonance, and the superscript is the resonance order (i.e., order of occurrence; first, second, or third for that particular principal mode number). The perfect sphere α_0 and Q values for these six resonances are given in Table 1.

Figure 1 provides the calculated magnetic wave resonance Q values for a N=20 corrugated particle as a function of surface perturbation amplitude (ϵ). As can be seen in Fig. 1, for each of the three magnetic wave resonances, the presence of the surface perturbation has a minimal influence on the resonance quality (Q) until a certain threshold value of surface perturbation amplitude (ϵ) is obtained. Beyond this threshold value, the resonance Q decreases with increasing ϵ. (The results for the three electric wave resonances, not shown here, were similar.) For the high-Q d^1_{97} resonance, the threshold ϵ value is about 2×10^{-6}, for the mid-Q d^2_{94} resonance the value is about 2×10^{-3}, and for the low-Q d^3_{91} resonance the value is about 1×10^{-3}.

To investigate the influence of N (the number of cycles of perturbations around the circumference of the particle) on the Q versus ϵ results, Q's were calculated with $\epsilon = 1 \times 10^{-3}$ for a range of N values from 20 to 40. The results for the three magnetic wave resonances are given in Fig. 3. As shown in Fig. 3, there is an apparent "grating" effect, with certain N and resonance mode combinations being (in a relative way) strongly Q-spoiling and others (in a relative way) weakly Q-spoiling. For the conditions of Fig. 2, the N=20 case was strongly Q-spoiling for the d^1_{97} resonance, weakly Q-spoiling for the d^2_{94} resonance, and strongly Q-spoiling for the d^3_{91} resonance.

In order to counteract the grating effect demonstrated in Fig. 3, calculations were

performed for a more irregular "combined" surface roughness particle where

$$\hat{r} = 1 + \frac{\epsilon}{\sqrt{3}}[-cos(18\theta) + cos(30\theta) + cos(42\theta)] \quad . \tag{17}$$

The Q versus ϵ results for the combined surface roughness particle are given in Fig. 4. (A cross section of the particle described by Eq. (17) is also shown in Fig. 4.) In comparing Fig. 4 with Fig. 2, it can be observed that for the combined surface roughness particle the threshold value of ϵ increases for the d_{97}^1 resonance, decreases (by over an order of magnitude) for the d_{94}^2 resonance, and stays approximately the same for the d_{91}^3 resonance.

In Ref. 12, Lai et al. suggest that the surface perturbation effect on resonance quality can be modeled in general using

$$1/Q = 1/Q_{sp} + C_1\epsilon + C_2\epsilon^2 + C_3\epsilon^3 + ... \tag{18}$$

where Q_{sp} is the Q for the perfect sphere. Lai et al.[12] also present arguments that the dominate term on the right-hand-side of Eq. (18) should be the second-order term so that,

$$1/Q \approx 1/Q_{sp} + C_2\epsilon^2 \quad . \tag{19}$$

Equation (19) was used with the calculated Q values at $\epsilon = 1 \times 10^{-3}$ to determine C_2 for each of the six different resonances (magnetic wave and electric wave) for both the N=20 corrugated particle and for the combined surface roughness particle. The results are presented in Table 1. For ten of the twelve cases, Eq. (19) was found to accurately model the Q versus ϵ results. This is demonstrated by the dashed lines of Figs. 2 and 4, which were evaluated using Eq. (19) along with the Q_{sp} and C_2 values of Table 1. The two exceptions were the d_{94}^2 and c_{94}^2 resonances for the N=20 corrugated particle. For these two cases, the surface perturbation effect was weakly Q-spoiling and the calculated C_2 values based on Eq. (19) were relatively small (see Table 1). For the N=20 corrugated particle d_{94}^2 resonance, the Q versus ϵ relationship was much better modeled retaining the fourth-order term, instead of the second-order term, such that $1/Q \approx 1/Q_{sp} + C_4\epsilon^4$ where $C_4 = 13{,}960$. This curvefit is shown by the dashed-dot line of Fig. 2. For the N=20 corrugated particle c_{94}^2 resonance, a modeling of the Q versus ϵ relationship required retaining both the second-order (C_2) and fourth-order (C_4) terms. In general, it appears that Eq. (19) is an appropriate model for most conditions, the exceptions being those cases which are weakly Q-spoiling, in which case the fourth-order term must also be included.

4. Surface Perturbation Effects on Focused Beam Resonance Excitation

In order to investigate the effects of surface perturbations on the excitation localization principle, calculations were performed assuming focused beam, instead of plane wave, illumination. A linearly polarized fundamental Gaussian (i.e., TEM_{00} mode) beam propagating in the z-axis direction ($\theta_{bd} = 0°$) with a beam waist diameter such that $\alpha\tilde{w}_0 = 12.2122$ (e.g., a $2w_0 = 2\ \mu m$ beam waist diameter at $\lambda_{ext} = 0.5145\ \mu m$) was assumed. The fifth-order corrected Gaussian beam model of Ref. 17 was used to the determine the required electromagnetic field components for the incident beam. For the magnetic wave (TE) resonances, the resonances are most efficiently excited with the incident electric field parallel to the surface of the particle.[7] Thus, for the magnetic wave resonances, the direction of the incident

electric field was oriented in the x-axis direction ($\phi_{bd} = 0°$) and the focal point of the beam was translated along the y-axis ($\tilde{x}_0 = 0$, $\tilde{z}_0 = 0$). For the electric wave (TM) resonances, the resonances are most efficiently excited with the incident electric field perpendicular to the surface of the particle, and the focal point of the beam was again translated along the y-axis, but now with the direction of the incident electric field in the y-axis direction ($\phi_{bd} = 90°$). For the off-center focused Gaussian beam calculations all m-mode terms contribute (not just the $|m|$=1 terms as was the case for the plane wave illumination of Sec. 3) so, consistent with the degenerate perfect sphere condition, $|c_l|^2$ and $|d_l|^2$ were appropriately used to indicate the energy of the particular resonance.

Figure 5 shows a plot of the relative energy of the 97th principle mode ($l = 97$), 1st azimuthal mode (m = 1) magnetic wave resonance versus focal point positioning ($\tilde{y}_0 = y_0/a$) for the perfect sphere ($\epsilon = 0$) and for N=20 corrugated particles of three different surface perturbation amplitudes. The data for the perfect sphere demonstrates the excitation localization principle where the focal point location for the maximum resonance excitation is located outside the surface of the sphere at a position approximately given by Eq. (1). (For the d^1_{97} resonance, $r_0/a = 1.24$.) However, the calculations indicate that the presence of even a small amount of surface roughness (in this case, $\epsilon = 1 \times 10^{-5}$ which, for a 12 micron diameter particle would correspond to a surface perturbation amplitude of less than one angstrom, which is smaller than one molecule of water), the position for maximum resonance excitation moves to a location just inside the surface of the particle. A similar effect was observed for all six types of resonances (magnetic and electric wave resonances of first, second, and third order) for the N=20 corrugated particle, the combined roughness particle described by Eq. (17), and various other N-valued corrugated particles. As an additional example, Fig. 6 shows the results for the combined surface roughness particle at the d^2_{94} resonance. For these conditions, the focal point location for maximum resonance excitation moves just inside the surface of the particle when the surface perturbation amplitude attains a value of about $\epsilon = 5 \times 10^{-4}$.

The general trend appears to be that when the surface perturbation amplitude is large enough to significantly reduce the Q of the resonance (e.g., see Figs. 2 and 4), then the focal point position for optimum resonance excitation shifts from the position outside the particle, as predicted by the excitation localization principle expressed by Eq. (1), to a position just inside the surface of the particle. Apparently, the same surface perturbations that are increasing surface scattering and lowering the Q of the resonance are also scattering the incident light so as to channel increased power into the resonance. From a mathematical viewpoint, as discussed in Sec. 3, the surface perturbations allow a cross-coupling of the incident field, internal field, and scattering field series coefficients, which, for a given mode resonance, provides both increased mechanisms for scattering (increased losses and a lowering of the resonance Q) and increased mechanisms for channeling incident power into the resonance (a shift of position of optimal resonance excitation to the surface of the particle).

The calculated results are consistent with the experimental observations of Ref. 9. For the quartz sphere, optimum resonance excitation always occurred at the surface of the particle, suggesting that the inherent surface roughness of the particle was, at least for the particular resonances investigated, greater than the threshold value. For the liquid droplet, optimum resonance excitation occurred according to Eq. (1) for the d^2_{94} and d^3_{91} resonances but occurred at the surface of the particle for the high-Q d^1_{97} resonance. According to

Fig. 4, this would suggest that the surface roughness amplitude of their droplets would lie somewhere between 2×10^{-5} (large enough to spoil the d_{97}^1 resonance) but below about 2×10^{-4} (not large enough to spoil the d_{94}^2 resonance). For the experimental conditions of Ref. 9 (water droplets with 0.5145 μm wavelength illumination), this would correspond to a surface roughness amplitude somewhere between approximately 1 and 10 angstroms.

5. Conclusions

The boundary matching method was systematically used to investigate the effects of surface perturbations on microsphere resonance Q and the excitation localization principle. For a given resonance mode, the presence of a distributed surface perturbation has a negligible effect on the resonance Q until a threshold value of surface perturbation amplitude (ϵ) is reached, after which the Q decreases with increasing ϵ. The Q as a function of ϵ relationship was found to follow the simple second-power model suggested by Lai et al.[12] for most cases, however, for conditions that were weakly-Q spoiling, it was found necessary to include an additional fourth-power term. The excitation localization principle was found to fail when the surface roughness amplitude is large enough to cause a significant lowering of the resonance Q. In this case, for focused beam excitation of the resonance, the resonance was found to be most efficiently excited with the focal point of the beam located at a position just inside the surface of the particle. Apparently, for these conditions, the internal resonance mode is being pumped predominately by surface scattering due to the presence of the surface perturbations.

Acknowledgment

This research was supported by the Naval Research Laboratory through Grant No. N00173-98-1-G008. The author expresses his appreciation to Anthony J. Campillo, Naval Research Laboratory, Washington, D.C., for our many discussions concerning the physical interpretations and implications of this work.

APPENDIX A

For a perfectly spherical particle with a relative index of refraction of 1.332 (no absorption), the first-order, 240th principal mode number, magnetic wave (TE) resonance (d_{240}^1) occurs at a size parameter of $\alpha_o = 2\pi a/\lambda_{ext} = 188.16400070000720377166$ with a resonance quality of $Q_o = 1.86 \times 10^{24}$.

REFERENCES

1. D.W. Vernooy, V.S. Ilchenko, H. Mabuchi, E.W. Streed, and H.J. Kimble, "High-Q measurements of fused-silica micropsheres in the near infrared," Opt. Lett. **23**, 247-249 (1998).

2. V. Lefevre-Seguin, M. Brune, J.M. Raimond, and S. Haroche, "Very high-Q whispering gallery mode resonances observed on fused silicon microspheres," Europhys. Lett. **23**, 327-334 (1993).

3. H-B. Lin, A.L. Huston, J.D. Eversole, and A.J. Campillo, "Double-resonance stimulated Raman scattering in micrometer-sized droplets," J. Opt. Soc. Am. B **7**, 2079-2089 (1990).

4. H-B. Lin and A.J. Campillo, "CW Nonlinear optics in droplet microcavities displaying enhanced gain," Phys. Rev. Lett. 73, 2440-2443 (1994).

5. M. Essien, J.B. Gillespie, and R.L. Armstrong, "Observation of suppression of morphology-dependent resonances in singly levitated micrometer-sized droplets," Appl. Opt. **31**, 2148-2153 (1992).

6. H.C. van de Hulst, *Light Scattering by Small Particles* (Dover Publications, Inc., New York, 1981).

7. J.P. Barton, D.R. Alexander, and S.A. Schaub, "Internal fields of a spherical particle illuminated by a tightly focused laser beam: Focal point positioning effects at resonance," J. Appl. Phys. **65**, 2900-2906 (1989).

8. E.E.M. Khaled, S.C. Hill, P.W. Barber, and D.Q. Chowdhury, "Near-resonance excitation of dielectric spheres with plane waves and off-axis Gaussian beams," Appl. Opt. **31**, 1166-1169 (1992).

9. H-B. Lin, J.D. Eversole, A.J. Campillo, and J.P. Barton, "Excitation localization principle for spherical microcavities," Opt. Lett., in press (1998).

10. J.P. Barton and D.R. Alexander, "Electromagnetic fields for an irregularly-shaped, near-spherical particle illuminated by a focused laser beam," J. Appl. Phys. **69** 7973-7986 (1991).

11. H.M. Lai, P.T. Leung, K. Young, P.W. Barber, and S.C. Hill, "Time- independent perturbation for leaking electromagnetic modes in open systems with application to resonances in microdroplets," Phys. Rev. A **41**, 5187-5198 (1990).

12. H.M. Lai, C.C. Lam, P.T. Leung, and K. Young, "Effect of perturbations on the widths of narrow morphology-dependent resonances in Mie scattering," J. Opt. Soc. Am. B **8**, 1962-1973 (1991).

13. A. Mekis, J.U. Nockel, G. Chen, A.D. Stone, and R.K. Chang, "Chaos and Q-spoiling in lasing droplets," Phys. Rev. Lett. **75**, 2682- (1995).

14. E. S-C. Ching, P-T. Leung, and K. Young, "The role of quasinormal modes," Chapter 1 in *Optical Processes in Microcavities*, R.K. Chang and A.J. Campillo, eds. (World Scientific, Singapore, 1996).

15. M.M. Mazumder, D.Q. Chowdhury, S.C. Hill, and R.K. Chang, "Perturbation effects on the resonances of a spherical dielectric microsphere," Chapter 6 in *Optical Processes in Microcavities*, R.K. Chang and A.J. Campillo, eds. (World Scientific, Singapore, 1996).

16. J.P. Barton, "Electromagnetic field calculations for a sphere illuminated by a higher-order Gaussian beam. I. Internal and near-field effects," Appl. Opt. **36**, 1303-1311 (1997).

17. J.P. Barton and D.R. Alexander, "Fifth-order corrected electromagnetic field components for a fundamental Gaussian beam," J. Appl. Phys. **66**, 2800-2802 (1989).

Table 1. Size parameters (α), quality factors (Q), and C_2 modeling constants for each of the six resonances for the perfect sphere, the $\epsilon = 0.001$ corrugated (N=20), and the $\epsilon = 0.001$ combined surface roughness particles.

resonance mode	α_{sp}	Q_{sp}	α_{20}	$C_{2,20}$	α_{comb}	$C_{2,comb}$
d^1_{97}	78.557854283	1.419E+09	78.5569	72.57	78.55996	10.57
d^2_{94}	81.2557685	1.207E+06	81.256966	0.014	81.2574	44.01
d^3_{91}	83.06530	1.159E+04	83.0645	34.49	83.066	16.07
c^1_{97}	79.018369252	1.007E+09	79.0200	52.77	79.02007	5.24
c^2_{94}	81.6683833	8.12E+05	81.66942	0.175	81.6696	20.27
c^3_{91}	83.40505	7.41E+03	83.4048	19.37	83.405	8.11

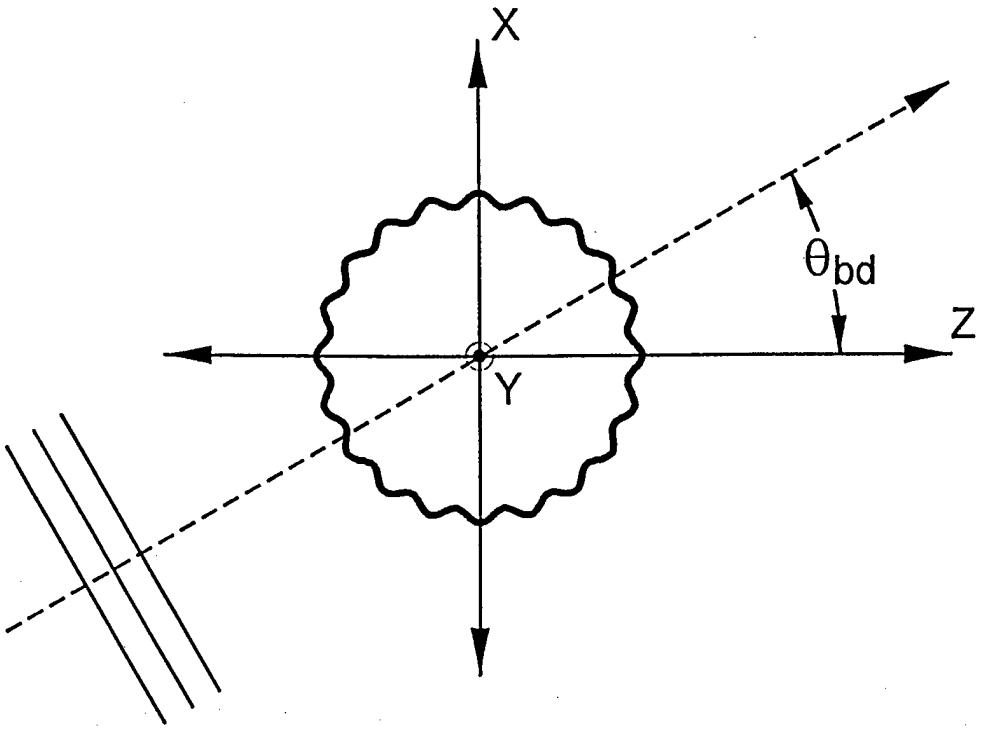

Fig. 1. Geometrical arrangement for the boundary matching method solution.

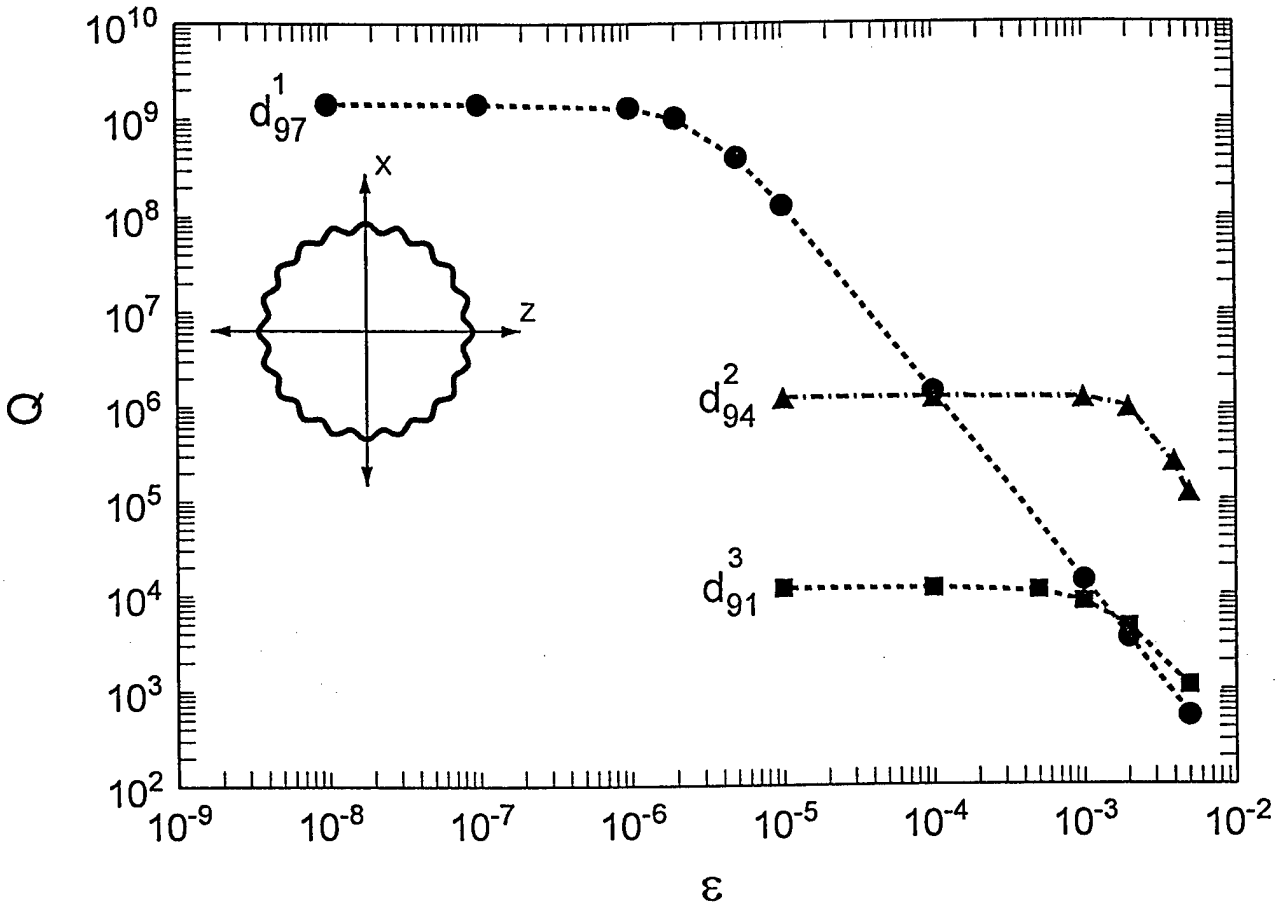

Fig. 2. Resonance quality (Q) as a function of perturbation amplitude (ϵ) for each of the three magnetic wave resonances. Corrugated particle with N $\doteq$ 20.

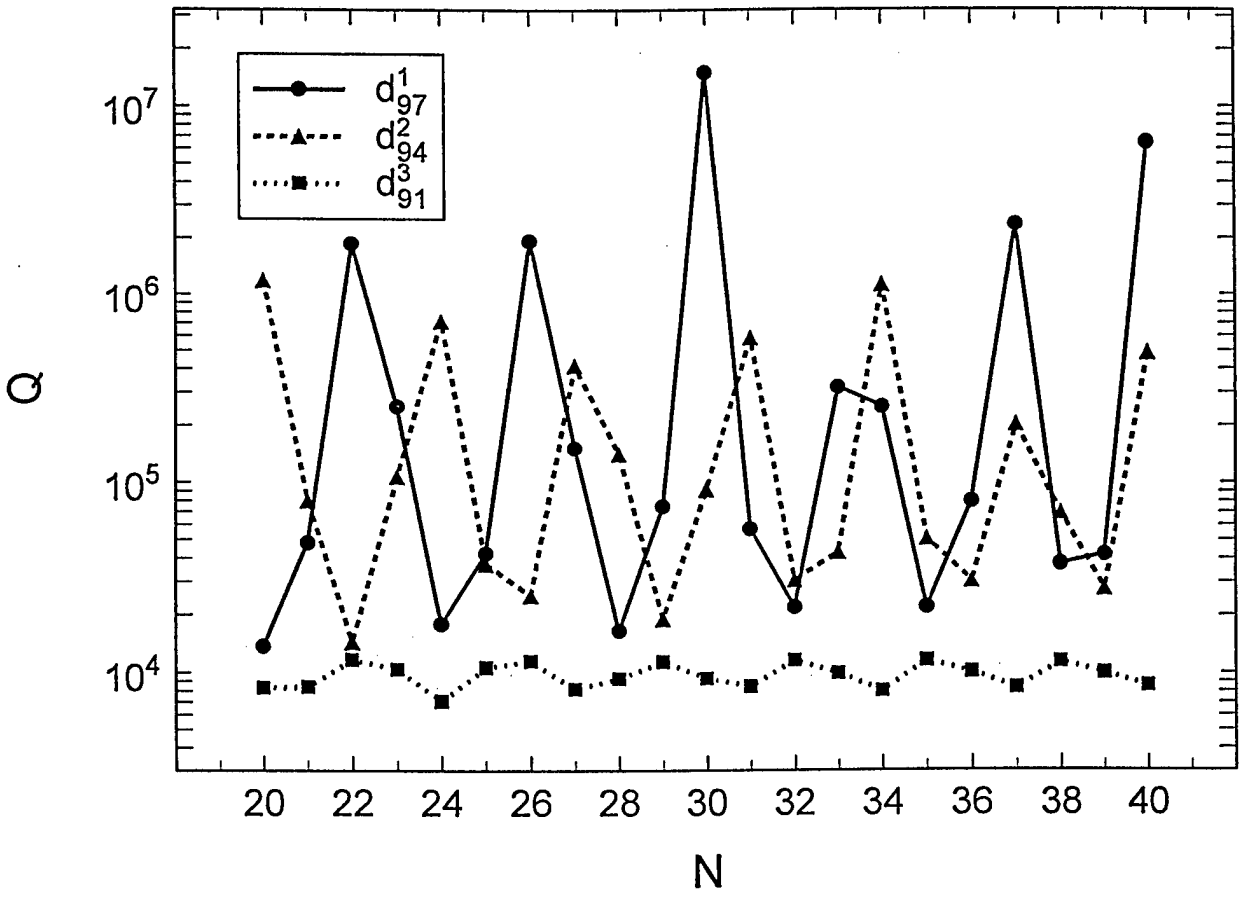

Fig. 3. Resonance quality (Q) as a function of N for each of the three magnetic wave resonances. Corrugated particle with $\epsilon = 0.001$.

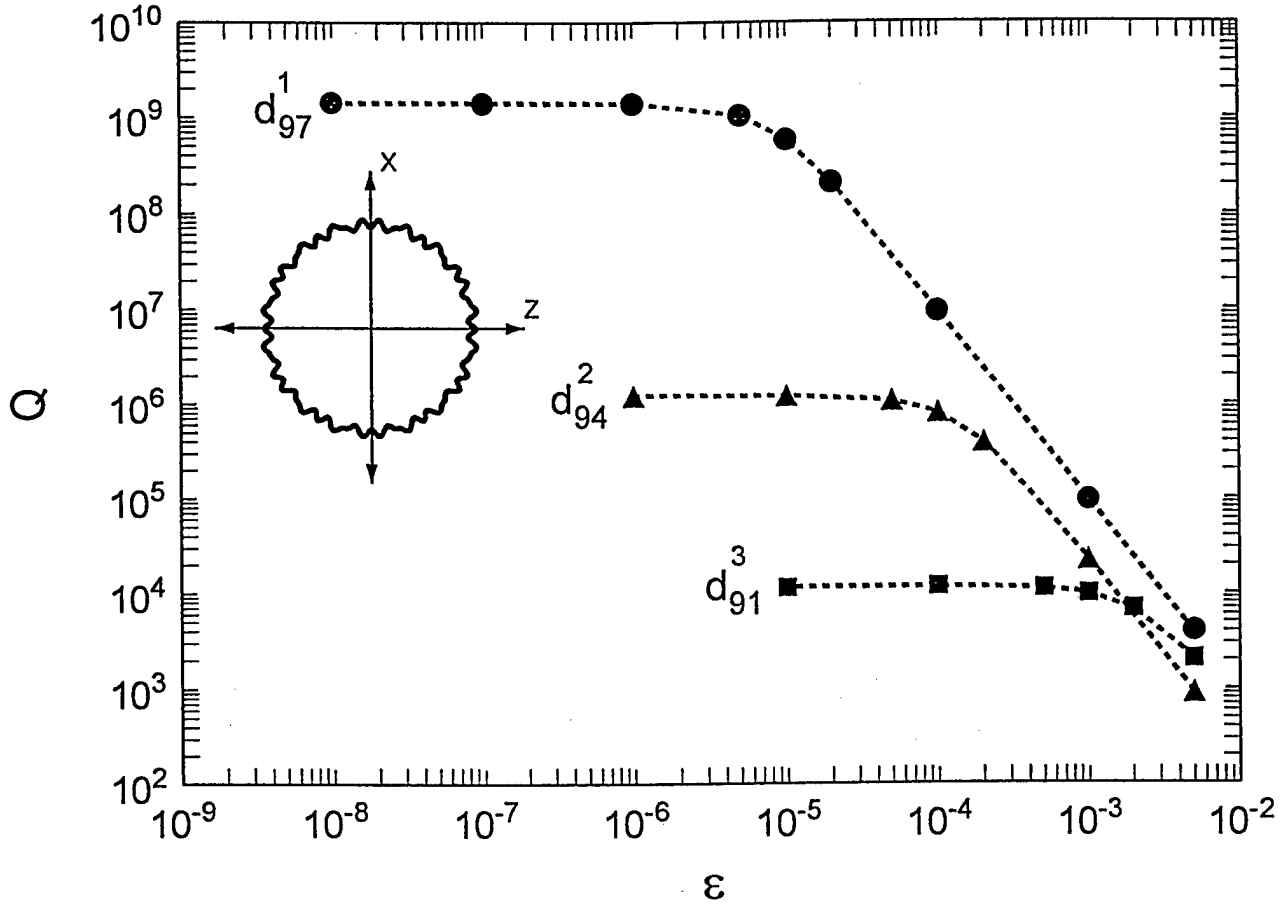

Fig. 4. Resonance quality (Q) as a function of perturbation amplitude (ϵ) for each of the three magnetic wave resonances. Combined surface roughness particle.

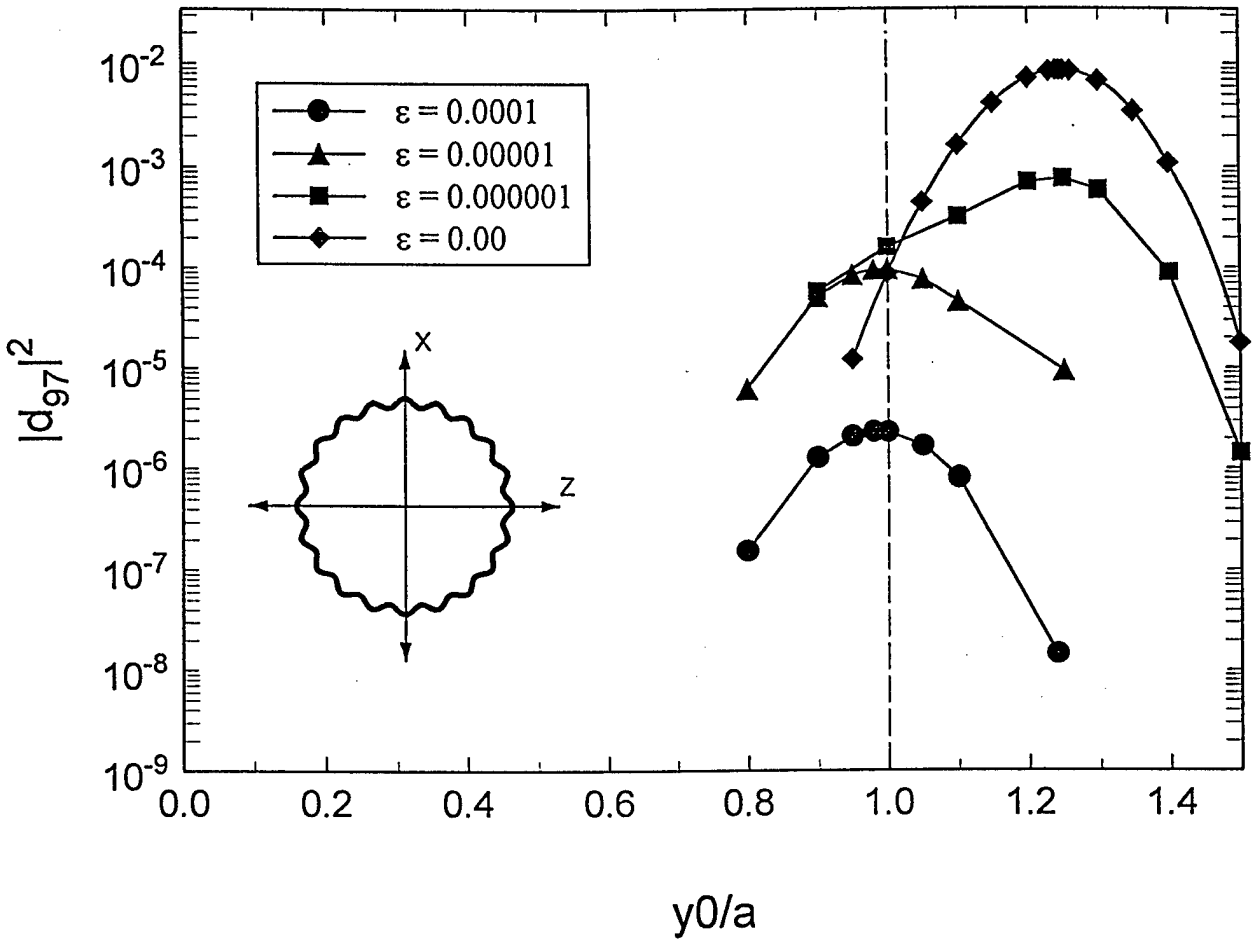

Fig. 5. $|d_{97}|^2$ as a function of incident beam focal point positioning (y_0/a) for $\epsilon = 0.00$, 0.0000001, 0.000001, and 0.0001. Corrugated (N=20) particle at the d^1_{97} resonance.

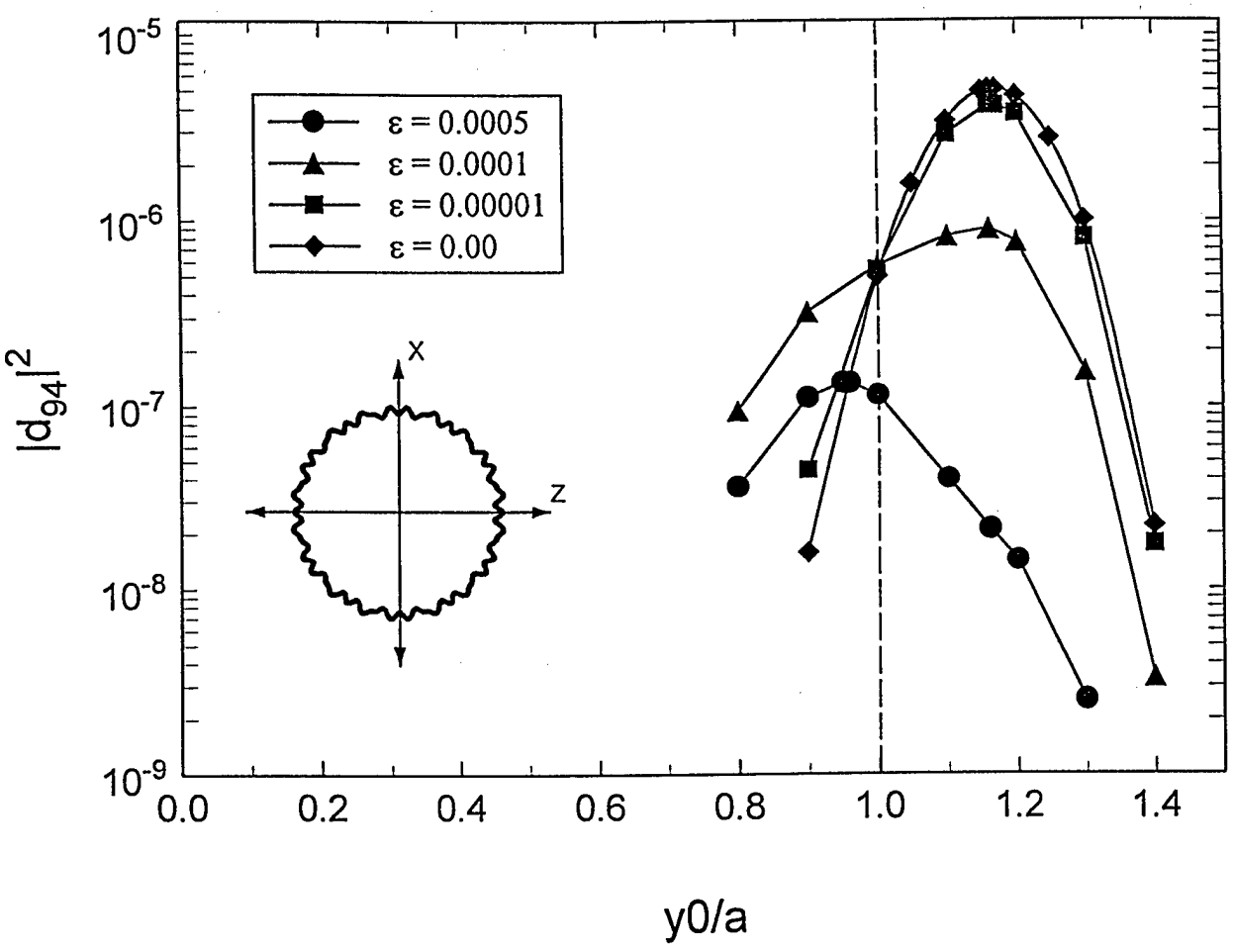

Fig. 6. $|d_{94}|^2$ as a function of incident beam focal point positioning (y_0/a) for $\epsilon = 0.00$, 0.00001, 0.0001, and 0.0005. Combined surface roughness particle at the d^2_{94} resonance.

REPORT DOCUMENTATION PAGE

Form Approved
OMB No. 0704-0188

1. AGENCY USE ONLY *(Leave blank)*	2. REPORT DATE	3. REPORT TYPE AND DATES COVERED
	15 March 1999	Final Report 18 May 98 - 31 Dec 98

4. TITLE AND SUBTITLE
Analysis of Resonance Excitation and Surface Distortion of Single Microdroplets using Focused Monochromatic Illumination

5. FUNDING NUMBERS
Grant No.
N00173-98-1-G008
PR No. 56-9117-98

6. AUTHORS
John P. Barton

7. PERFORMING ORGANIZATION NAME(S) AND ADDRESS(ES)
University of Nebraska-Lincoln
Sponsored Programs Office
306 Administration Building
Lincoln, NE 68588-0430

8. PERFORMING ORGANIZATION REPORT NUMBER
LWF/11-188-11401

9. SPONSORING/MONITORING AGENCY NAME(S) AND ADDRESS(ES)
Department of the Navy
Naval Research Laboratory
4555 Overlook Avenue, SW
Washington, DC 20375-5326

10. SPONSORING/MONITORING AGENCY REPORT NUMBER

11. SUPPLEMENTARY NOTES

12a. DISTRIBUTION/AVAILABILITY STATEMENT
Approved for Public Release

12b. DISTRIBUTION CODE

13. ABSTRACT *(Maximum 200 words)*

Theoretical procedures were developed, computer programs were written, and systematic calculations were performed to investigate (1) the validity of van de Hulst's localization principle for focused laser beam resonance excitation of spherical and nonspherical particles and (2) the effects of laser beam induced electromagnetic stresses on droplet geometry.

14. SUBJECT TERMS
Mie scattering, localization principle, electromagnetic stress, laser/droplet interaction

15. NUMBER OF PAGES
34

16. PRICE CODE

17. SECURITY CLASSIFICATION OF REPORT	18. SECURITY CLASSIFICATION OF THIS PAGE	19. SECURITY CLASSIFICATION OF ABSTRACT	20. LIMITATION OF ABSTRACT